INSTITUTE OF PHYSICS PUBLISHING JOURNAL OF PHYSICS: CONDENSED MATTER

J. Phys.: Condens. Matter **14** (2002) 7165–7176 PII: S0953-8984(02)35153-1

Laser deposition of thin films from $La_{0.7}Ca_{0.3}MnO_3$ targets prepared by sol–gel and solid-state methods

H Huhtinen, J Raittila, P Paturi, J Salminen and V S Zakhvalinskii

Wihuri Physical Laboratory, Department of Physics, University of Turku, FIN-20014 Turku, Finland

E-mail: hannu.huhtinen@utu.fi

Received 22 March 2002
Published 17 July 2002
Online at stacks.iop.org/JPhysCM/14/7165

Abstract

The sol–gel (SG) method is used to synthesize $La_{0.7}Ca_{0.3}MnO_3$ nanopowders having mean particle thickness of 1.3 nm. Targets for pulsed laser deposition of thin films are made from this material and compared with targets sintered from micron-size powder prepared by a typical solid-state (SS) method. Emission line intensity ratios observed from the laser plume give evidence that the paths of atomic species deposited from the SS target are clearly longer. The sizes of the particles in the SG plume are smaller than in the SS plume and agree with the particle sizes in the corresponding targets. According to x-ray photoelectron spectroscopy the deposited films have on the surface some excess of Ca and deficiency in Mn. The composition of the films prepared from the SG target is closer to ideal than the composition of the films made from the SS target. The SG films have a steeper magnetic transition and smoother surface than the SS films. Therefore the SG material is better suited for deposition of smooth thin films.

1. Introduction

Since the discovery of the colossal-magnetoresistance (CMR) phenomenon in manganese oxide perovskites [1–3], their magnetic and transport properties have been widely studied [4–7]. The main goals of these investigations have been physical models of the magnetotransport properties and achieving usefulness of these materials in device applications. It is well documented that structural, magnetic and magnetotransport properties of the manganites depend critically on the composition, growth conditions and microstructure of the material [8]. Even though pulsed laser deposition (PLD) is an established preparation method for stoichiometric multicomponent $La_{1-x}Ca_xMnO_3$ (LCMO) films [4, 9, 10], details of the interaction with the laser beam and the deposition target have not been investigated. When the target is made from a powder obtained with the typical high-temperature ceramic method the final grain size is of the order of 100 nm or larger. However, in many applications a powder with smaller grain size would

Table 1. Metallic compositions of the SS and SG targets and ideal $La_{0.7}Ca_{0.3}MnO_3$, obtained by AAS.

Species (%)	Ideal LCMO	SS target	SG target
La	35	33.3	34.1
Ca	15	14.6	15.6
Mn	50	49.6	49.8

be of advantage [10–14], e.g. when very smooth structures for studying spin-polarized current transport are needed [15]. Because the particle size increases by thermal agglomeration when the preparation temperature is increased, alternative synthesis routes using lower annealing temperatures are required.

In this work we investigate the influence of the powder synthesis, either solid-state (SS) or sol–gel (SG) reaction, on physical properties of the PLD target for growth of LCMO films. The composition and size of the particles in the laser plume are investigated by optical emission spectroscopy (OES) and by atomic force microscopy (AFM). The phase formation and surface structure of the films are investigated using x-ray photoelectron spectroscopy (XPS), AFM and magnetometry.

2. Preparation and characterization of the targets

The material of the SS target is made by calcining a stoichiometric mixture of high-purity La_2O_3, $CaCO_3$ and MnO_2 salts for 35 h at 1320 °C in air, with intermediate grindings. Then the powder obtained is pressed into a pellet and sintered for 22 h in air at 1375 °C. The density of the SS target is 4.96 g cm^{-3} as determined by its volume and weight.

For the SG reaction, water solutions of the metal nitrates are mixed in the ratio of 0.7:0.3:1 = [La]:[Ca]:[Mn] for the metallic ions [14]. The concentrations of the solutions are determined by comparing their density with published data (wt%) [16]. Then the required amount of 10 × ([La] + [Ca] + [Mn]) urea is added to the solution which is slowly heated to 150 °C. On cooling back to room temperature a pink gel is obtained. This gel is fired in an oven at 250 °C for 3 h in air to obtain a precursor, which is calcined for 5 h at 600 °C and 5 h at 800 °C in air with intermediate grindings. Using the pressure of 1500 kg cm^{-2} the powder is pressed into a pellet of 2 cm diameter and sintered for 6 h at 1175 °C in air. The density of the SG target is 3.22 g cm^{-3}.

The chemical compositions of both targets, determined by atomic absorption spectroscopy (AAS), are compared with the composition of ideal $La_{0.7}Ca_{0.3}MnO_3$ in table 1. Although the deviations from the nominal values are not large, the composition of the metallic compounds is found to be in the SG target higher and closer to the nominal values than in the SS target, indicating more impurities in the SS target.

The XRD patterns collected within the range of $2\theta = 20°$–$90°$ using the angular step of 0.02° show that the diffraction peaks from the SS target are narrower and better resolved than the peaks from the SG target. This indicates that the crystallites of the SG target are smaller. Applying the Scherrer formula [18], the average particle sizes are $D_{SG} = 46$ nm and $D_{SS} = 128$ nm for the SG and the SS targets, respectively, giving $D_{SG}/D_{SS} = 0.36$. The values obtained for the SG powder are close to those determined by XRD and transmission electron microscopy [11, 12, 14].

The samples for AFM were prepared by ultrasonic spraying of a suspension of calcined SG powder in ethanol on a polished crystalline silicon (100) plate. The particle size distribution obtained from the AFM images is shown in figure 1. The mean particle height and the radius calculated from these distributions are $h_{SG} = 1.3$ nm and $r_{SG} = 90$ nm, respectively.

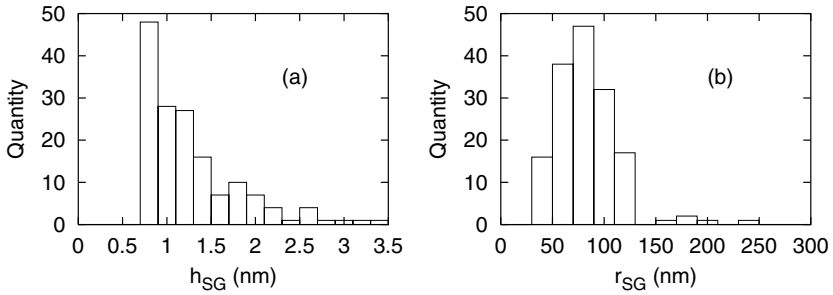

Figure 1. Distributions of the height (a) and the radius (b) of the SG particles imaged by AFM. The total number of particles analysed is 160.

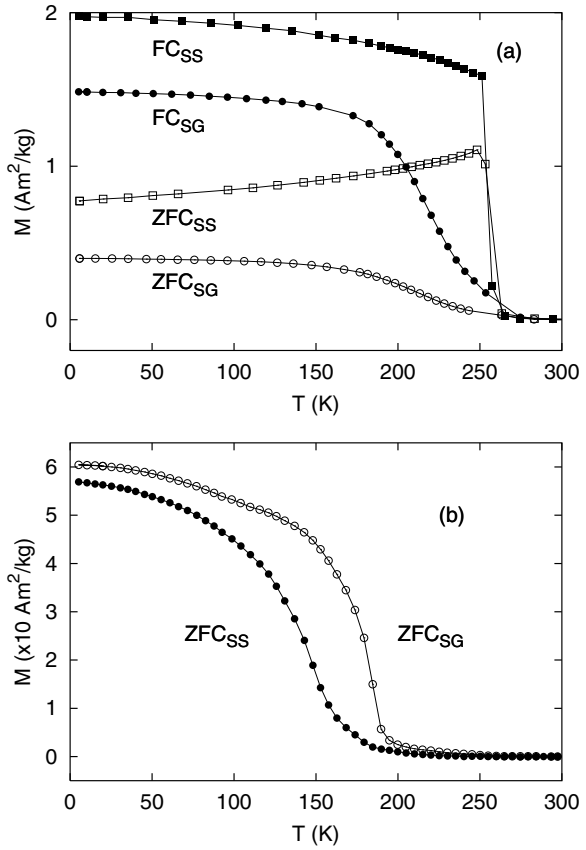

Figure 2. Temperature dependences of M_{FC} and M_{ZFC} for the SS (■ and □) and the SG targets (● and ○), respectively (a) and the behaviour of $M_{ZFC}(T)$ in the SS and SG films deposited on a $SrTiO_3$ substrate at the temperature $T_s = 780\,^{\circ}C$ (b) (see section 4). The measurements were made in fields of 1 mT (targets) and 8 mT (films) using a SQUID magnetometer.

The temperature dependence of the field-cooled (M_{FC}) and zero-field-cooled (M_{ZFC}) magnetizations of small pieces cut from the SS and SG targets are shown in figure 2(a). In the case of the SS target the ZFC and FC curves exhibit a sharp ferromagnetic (FM) transition and diverge clearly below the Curie temperature T_C. The magnetization data for the SG target

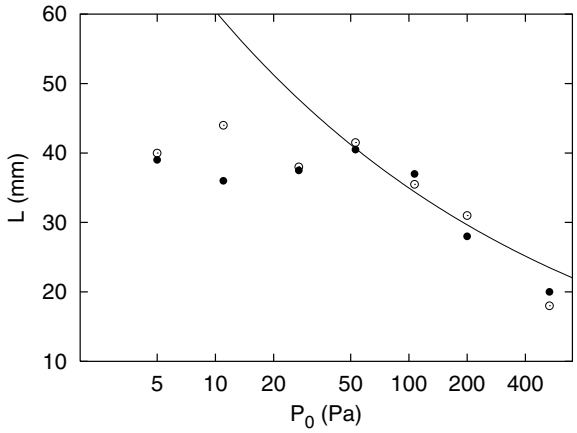

Figure 3. Dependences of the length of the plume on the oxygen pressure for the SS target (dots) and SG target (open circles) obtained from the CCD photographs. The solid curve is a fit of equation (1) with experimental data on L valid for $P_0 > 50$ Pa.

show a much broader FM transition, suggesting a distribution of T_C in the grains of the target. This effect may be, at least in part, attributed to variation of the hole concentration, i.e. the ratio Mn^{3+}/Mn^{4+}, in the perovskite structure of the SG target [19].

The magnetization of the SG target is smaller than that of the SS target. Since no spurious phases are observed in the XRD data, the smaller M can be attributed to smaller effective grain size due to a larger amount of amorphous component in small grains [11].

3. Investigations of the plume

3.1. Size and shape of the plume

The laser-driven plume was generated by a pulsed XeCl excimer laser working at $\lambda = 308$ nm, the pulse duration of $\tau = 25$ ns and the operation frequency of 10 Hz. The laser beam was focused with an incidence angle of 45° relative to the surface of the rotating target. During ablation the oxygen pressure in the stainless steel deposition chamber was $P_0 = 35$ Pa and the laser energy per pulse was $E = 110$ mJ corresponding to the fluence of 2 J cm^{-2} over a spot $S = 5$ mm^2 on the surface of the target.

The shape and the structure of the plume were imaged with a time-resolving charge-coupled-device (CCD) camera through a window on top of the deposition chamber. The plume, which is symmetric around the normal to the target, has a bright plasma cloud with a pronounced glow near the surface of the target. Close to the target the plume expands in a conical shape but is almost spherical far from it. The plume from the SG target is brighter and narrower than the plume from the SS target. The light emission intensity and the length of the plume, L, decrease when P_0 is increased.

As shown in figure 3 the dependences of L on P_0 are almost the same for the SS target (dots) and the SG target (open circles). Below 50 Pa L is independent of P_0, attaining the maximum value of 40 mm which is also the maximum deposition distance. Assuming that the cloud of high-pressure ablation products expands adiabatically, the experimental data on $L(P_0)$ for $P_0 > 50$ Pa can be well fitted (solid curve) with an expression [20]

$$L = B[(\gamma - 1)E]^{1/3\gamma} P_0^{-1/3\gamma} V_i^{(\gamma-1)/3\gamma}, \tag{1}$$

Table 2. Emission line intensity ratios I_{SG}/I_{SS} of different species in the plume from the SG and SS targets. The values in the third column are mathematical averages over the distance of $d = 3$–30 mm from the target. In the fourth column the intensity ratios are given at the deposition distance of 30 mm.

Species	Wavelength (nm)	I_{SG}/I_{SS} (average)	I_{SG}/I_{SS} (30 mm)
Ca(I)	445.48	0.95	0.25
Ca(II)	396.85	1.53	0.27
La(I)	545.51; 593.06	0.69; 0.64	0.46; 0.45
La(II)	407.73; 412.32	0.90; 1.07	0.26; 0.26
Mn(I)	403.08	1.19	0.30
LaO	441.8	0.99	0.24
MnO	558.5	1.00	0.52

where E is the energy of the laser pulse, $V_i \approx v_0 \tau S$ is the volume of the plasma, with $v_0 = 1 \times 10^6$ cm s^{-1} [21–23], $\tau = 25$ ns and S is the size of the light spot on the target. For a conical plume with a spherical end [20],

$$B = \left(1 + \frac{1}{\tan\phi}\right)\left[\frac{3\tan\phi}{\pi + 2\pi\tan\phi}\right]^{1/3}, \tag{2}$$

where the expansion angle ϕ is 25°, as determined from the CCD images. For the fitting parameter γ which is the ratio of the specific heats of the plume gas, we get $\gamma = C_p/C_v = 1.55$ close to the value for ideal gases [21, 22, 24, 25]. In the expansive stage (shock wave propagation), the front of the plume extends into a region where its pressure exceeds that of the external gas [26–28]. Once these pressures are equal, the ejected particles are transported to the substrate by diffusion [29–31].

3.2. Light emission from the plume

Light emission spectra of the plume between $\lambda = 300$ and 600 nm were observed at distances of $d = 3, 6, 10, 20, 30$ mm from the target using a 25 cm Ebert monochromator followed by a fast photomultiplier tube and a digital oscilloscope synchronized with the XeCl laser pulses. In figures 4(a) and (b) we show the intensities of the Ca(I), Ca(II), La(I), La(II), Mn(I), LaO and MnO emission lines [16, 32, 33] as a function of d for the SS and SG plumes. The intensities of the ionized atom emission lines reach a maximum at about $d = 10$ mm in both cases. The explanation for this maximum lies in the fact that in addition to atoms and molecules the laser pulse removes larger hot particles from the target [23, 34–36]. While flying in the plume these particles decompose to atomic species, reaching their maximum number at d corresponding to the maximum emission line intensity. In both plumes the relative amount of La increases at larger d. The relative intensities of the Ca emission lines from the SG target are smaller at large distances than the corresponding intensities from the SS target. The average emission line intensity ratios over the distance $d = 3$–30 mm for the SG and SS targets and the respective ratios at $d = 30$ mm are shown in table 2. The values of I_{SG}/I_{SS} at $d = 30$ mm are remarkably below the average, giving evidence that the path of the atomic species deposited is much longer from the SS target than from the SG target.

A cloud of material, which absorbs laser light because of the photoionization and the inverse Brehmsstrahlung processes, is formed near the surface of the target. The absorbed energy increases the temperature of the plume and leads to a faster expansion until the plume is in thermal equilibrium. The ratio of the densities of the ionized and the neutral species, n_i

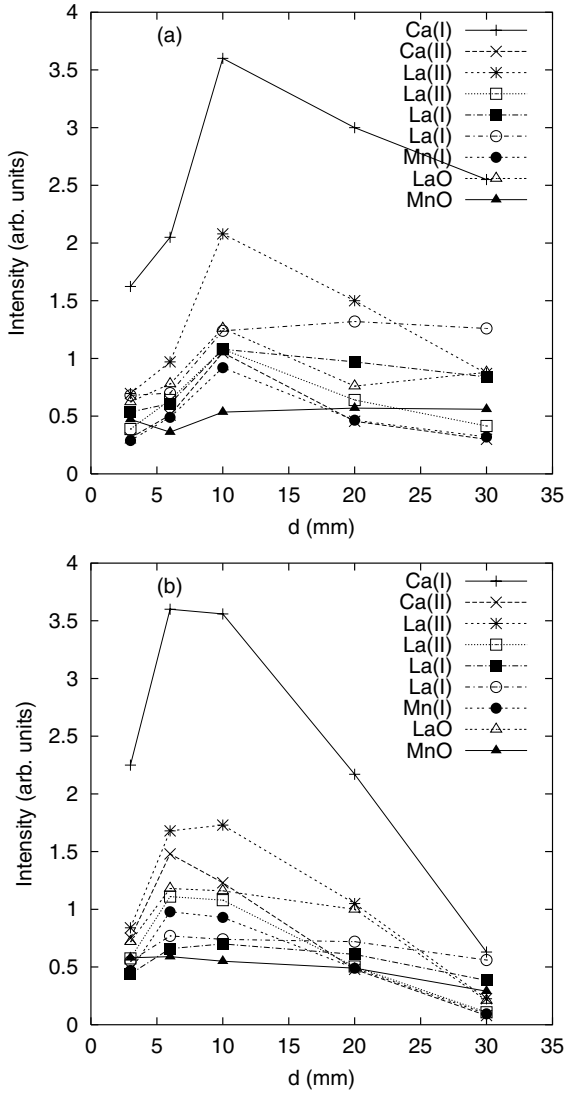

Figure 4. Emission line intensities observed at various distances from the surface of the SS target (a) and the SG target (b): Ca(I) (+: 445.48 nm), Ca(II) (×: 396.85 nm), La(I) (■: 545.51 nm, ○: 593.06 nm), La(II) (∗: 407.73 nm, □: 412.32 nm), Mn(I) (●: 403.08 nm), LaO (△: 441.8 nm), MnO (▲: 558.5 nm).

and n_n, respectively, can be obtained from the Saha's equation [37]

$$\frac{n_i}{n_n} = \kappa \frac{T^{3/2}}{n_i} \mathrm{e}^{-E_i/kT}, \tag{3}$$

where E_i is the first ionization energy and $\kappa = 2.4 \times 10^{15}$ is a constant [38]. The temperature of the plume, T, can be determined from the experimental formula [34]

$$T(x) = 1324\ \mathrm{K\ cm^{-1}} \times x^{-0.8} + 2089\ \mathrm{K}, \tag{4}$$

where x is the distance of the front of the expanding plume from the target. Using the expression

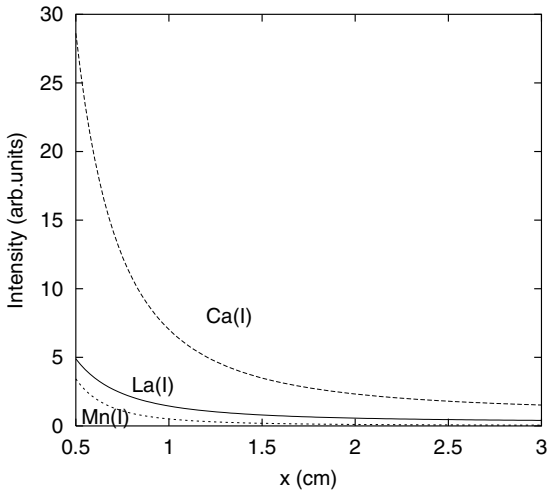

Figure 5. Relative intensities of the ionized species in the laser plume I_{ik}, calculated from equation (7) for La (solid curve), Ca (dashed curve) and Mn (dotted curve).

$n_n = n - n_i$, where n is the total particle density, we solve equation (3) for the relative densities of the ionized species as a function of x:

$$\frac{n_i}{n} = \frac{1}{2n}\left[\sqrt{\alpha^2(x) + 4n\alpha(x)} - \alpha(x)\right], \tag{5}$$

where $\alpha(x) = \kappa T^{3/2}(x) \exp[-E_i/kT(x)]$. The total particle density n can be estimated from

$$n = \frac{N}{V} = \frac{N}{\frac{4\pi}{3}ab^2}, \tag{6}$$

where N is the total number of particles and a and b are the semiaxes of the plume ellipsoid. The ratio of a and b can be determined from the CCD images as $b/a = 0.67$ and the total number of the particles can be estimated as [39, 40] $N = 10^{15}$. The observable intensities I_{ik} are calculated from

$$I_{ik} = A_{ik} n_i, \tag{7}$$

where A_{ik} is the spontaneous emission probability of the species. Using equations (4)–(7), the ionization energies E_i (5.61 eV for La, 6.11 eV for Ca and 7.43 eV for Mn)[16] and the emission probabilities A_{ik} (7.6×10^2, 8.6×10^3 and 5.78×10^3, respectively)[17], we can calculate the emission intensities for La(I), Ca(I) and Mn(I). As shown in figure 5 the intensity of Ca(I) should be highest and the intensities of Mn(I) and La(I) should be effectively the same. This agrees well with our experimental results in figure 4.

When La, Ca and Mn atoms travel through the background O_2 gas they can be oxidized according to the reaction $X + O_2 \rightarrow XO + O$, in line with the data in figure 4 where the LaO and MnO emission intensities remain relatively high at large d. In table 3 we show the bond dissociation energies in diatomic molecules, D_{XO}, and their changes, ΔD, in oxygen [16]. Because of the high exothermicity and bond dissociation energy, La is oxidized very easily resulting in enhancement of the LaO emission intensity in the O_2 ambient. The reaction of Mn with O_2 is expected to be less effective because of the low bond dissociation energy and negative exothermicity of MnO. The relative intensities of LaO and MnO are also higher in the SS plume than in the SG plume at $d = 30$ mm. It is possible that the reaction Ca + O_2

Table 3. Bond dissociation energies of diatomic molecules, D_{XO}, and the exothermicities, ΔD, of the chemical reaction $X + O_2 \rightarrow XO + O$ [16].

X (eV)	O	Ca	Mn	La
D_{XO}	5.16	3.65	4.17	8.16
ΔD	0	−1.51	−0.99	3.0

Table 4. Average values of the height, h, and the diameter, D, of the particles captured in the plume at different distances d for the SS (left value) and the SG target (right value).

d (mm)	h (nm)	D (nm)	h/D
10	2.4/4.6	161/238	0.015/0.019
25	4.7/1.8	219/181	0.021/0.010
41	4.0/1.6	165/143	0.024/0.011
59	1.6/1.7	175/149	0.009/0.014

produces diatomic oxide molecules in the gas phase, but the exothermicity of the reaction is insufficient to generate electronically excited CaO.

3.3. Particles in the plume

For AFM investigation a proportion of the particles were captured on four sector-shaped silicon (100) plates located inside the plume at distances $d = 10, 25, 41, 59$ mm from the target. In figures 6(a) and (b) we plot the distributions of the average volumes of the particles, $V_a = \frac{\pi}{4} h D^2$, as a function of their height, h, and width, D, determined by AFM at different d. As can be concluded from figure 6(b) and from the values of D in table 4, the particles deposited from the SG target are big near the target but their size decreases rapidly with increasing d up to 25 mm, so the thickness of the particles at the normal deposition distance of 35 mm is only 1.7 nm. For the SS target, V_a is largest at $d = 40$ mm in the centre of the plume and at $d = 25$ mm when the distance l is 25 mm. The particles are thicker than 4 nm for d between 25 and 41 mm and have a tendency to grow when going from the centre of the plume towards the surface. According to the theory of nucleation during expansion of the plume, the agglomeration and condensation of the clusters is determined by a combination of temperature and vapour pressure in the background O_2 gas [41–43]. As shown by the AFM images, the average ratio of the heights of the particles deposited from the SG and the SS targets at $P_0 = 0.25$ Torr and $d = 35$ mm is $h_{SG}/h_{SS} = 0.4$. This value is approximately the same as the ratio of the grain size calculated from the XRD data for the targets.

4. Analysis of the films

The films were deposited from the SS and SG targets on $SrTiO_3$ substrates under the oxygen pressure $P_0 = 35$ Pa varying the temperature of the substrate, T_s, between 600 and 780 °C (maximum temperature available). The optimal deposition distance was found to be 35 mm, corresponding to the situation when the tip of the weak external part of the plume comes near the substrate. In figure 7 we show AFM images of the SS (a) and the SG (b) films and in table 5 we give the values of the surface rms roughnesses determined over five randomly selected areas of size $80 \times 80\ \mu m^2$ on the films. Clearly the value of $T_s = 600$ °C is too low for deposition of smooth films from both targets. The SG films deposited at $T_s = 780$ °C have the average rms roughness of only 2.3 nm and are smoother than any of the SS films. The surface density of

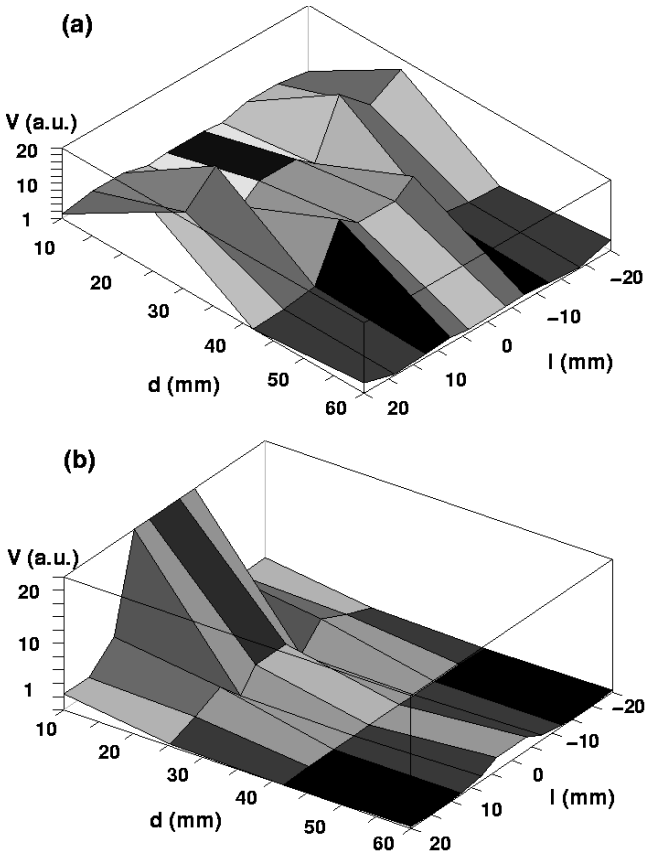

Figure 6. Distributions of the particle volumes in the plume emitted from the SS (a) and SG (b) targets, as functions of d and the distance from the symmetry axis of the plume, l.

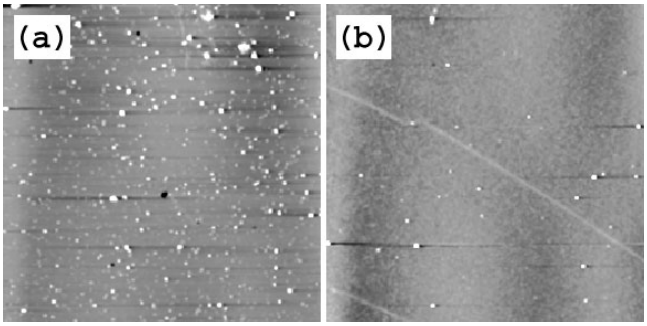

Figure 7. AFM images of the SS (a) and the SG (b) films deposited at $T_s = 780\,^{\circ}$C. The area of the images is $80 \times 80\ \mu m^2$ and the greyscales give the height variation of 20 nm.

the droplets, being only $0.03\ \mu m^{-2}$ over the area of $80 \times 80\ \mu m^2$, is about five times smaller on the SG films and their average size is also smaller (mean height for the SG film 19 nm and for the SS film 26 nm), as shown in figure 7.

The data on the composition of the surface of the films determined by XPS before and after Ar-ion sputtering are given in table 6. Clear excess of Ca and deficiency in Mn are observed

Table 5. The rms surface roughness and the Curie temperature T_C for the SS and SG films deposited on $SrTiO_3$ substrates at different temperatures T_s.

T_s (°C)	rms roughness (nm) SS/SG	$T_{C,onset}$ (K) SS/SG	$T_{C,derivative}$ (K) SS/SG
600	12.61/14.85	220/220	104/163
650	3.22/4.46	250/240	104/179
700	9.94/4.99	220/240	102/179
750	4.36/3.48	225/245	128/184
780	6.06/2.28	225/190	143/136

Table 6. Metallic concentrations of the LCMO films observed by XPS before and after sputtering the samples with Ar ions.

Sample	Sputtering time (min)	La (%)	Ca (%)	Mn (%)
Nominal		35	15	50
SS film	0	33.1	30.9	36.0
	1	46.8	11.5	41.7
	5	47.8	10.2	42.0
SG film	0	32.6	22.9	44.5
	1	48.2	10.1	41.7
	5	50.3	8.6	41.1

in both cases but this is more pronounced on the surface of the SS film. After sputtering for 5 min at the rate of 2 nm min^{-1}, the compositions of the films are found to be similar to but different from the compositions of the targets (see table 1). Because of possible preferential sputtering it is impossible to say whether the real compositions of the films after sputtering are the same as the compositions of the targets. However, it can be deduced that the compositions of the SS and the SG films differ on the surface from each other but not below it, because the relative concentrations stay almost the same when the sputtering time is increased. We should emphasize that the compositions found on the surface may not be affected by preferential sputtering, and that the surface of the SG film is closer to nominal than the surface of the SS film. These results agree well with the emission line intensities (figure 4), where the Ca(I) line intensity is higher at typical deposition distances in the SS than in the SG plume.

The magnetizations of the films (figure 2(b)) show FM ordering below the onset temperature T_{Co}, which is slightly lower than observed usually at the Ca concentration of 0.3 [3]. At high deposition temperatures the value of T_{Co} remains the same in the SS film, being slightly smaller in the SG film. The FM transitions are clearly steeper in the SG films than in the SS films. The value of T_C, defined as a peak in the magnetization derivative $\mathrm{d}M(T)/\mathrm{d}T$, is much higher in the SG (184 K) than in the SS films (143 K). In the SS films deposited at low T_s, the transition occurs in two steps indicating that there is a small amount of material which has higher T_C. This phenomenon disappears and the transition is sharpest when the optimal deposition temperature 780 °C is used.

The FM transition temperatures are substantially lower in the SG and the SS films than in the targets and the transition is much broader in the SS films than that in the SS target. The broadening of the transition in the films may result from the spread of different FM regions caused by chemical disorder, nonuniform distribution of Mn^{3+} and Mn^{4+} pairs and local oxygen stoichiometry [19, 44, 45]. In the manganese perovskites, T_C varies with the oxygen content, and thus the deviation of the oxygen stoichiometry at the surface appears to be negligible [46]. It is also known that the films post-annealed in air, N_2 or O_2 have higher magnetization and

higher T_C than as-grown films [1, 4].

5. Conclusions

Preparation of $La_{0.7}Ca_{0.3}MnO_3$ films by laser deposition from targets made with the SG and the SS methods is investigated. Data on the chemical compositions and structural properties show that the SG target is purer and more homogeneous than the SS target. The basic fragments in the SG target are flakes having average thickness of 1.3 nm and radius of 90 nm. The particle size ratio for the SG and SS targets measured by XRD is $D_{SG}/D_{SS} = 0.36$.

The atomic species evaporated from the SG and SS targets, as investigated by OES for the two targets, are quite similar, with the exception of excess Ca at normal deposition distance ($\approx$30 mm) in the case of the SS target. The paths of the atomic species deposited from the SS target are much longer, indicating higher kinetic energy and temperature of the particles at the distance of 30 mm along the axis of the plume. AFM investigations show that the average ratio of heights of the particles in the plume at the distance of 35 mm is $h_{SG}/h_{SS} = 0.4$.

According to XPS measurements, the films ablated from the SG and SS targets have a surface layer rich in Ca and deficient in Mn but reveal deeper in the film compositions closer to that of ideal material. The AFM investigations give evidence that, using optimized ablation parameters, the SG films are smoother than the SS films. Also the FM transitions are steeper and the Curie temperature higher in the SG films than in the SS films. On basis of this study we conclude that the SG material provides clear advantages in PLD of thin LCMO films.

Acknowledgments

We wish to thank Professor R Laiho for fruitful discussions and Dr K Laajalehto and Mr T Heikkilä for the XPS and XRD scans. The Wihuri Foundation and the Academy of Finland are acknowledged for financial support.

References

[1] von Helmholt R, Wecker J, Holzapfel B, Schultz L and Samwer K 1993 *Phys. Rev. Lett.* **71** 2331
[2] Chahara K, Ohno T, Kasai M and Kozono Y 1993 *Appl. Phys. Lett.* **63** 1990
[3] Schiffer P, Ramirez A P, Bao W and Cheong S W 1995 *Phys. Rev. Lett.* **75** 3336
[4] Ju H L, Kwon C, Li Q, Greene R L and Venkatesan T 1994 *Appl. Phys. Lett.* **65** 2108
[5] McCormack M, Jin S, Tiefel T H, Fleming R M and Phillips J M 1994 *Appl. Phys. Lett.* **64** 3045
[6] Xiong G C, Li Q, Ju H L, Mao S N, Senapati L, Xi X X, Greene R L and Venkatesan T 1995 *Appl. Phys. Lett.* **66** 1427
[7] Fontcuberta J 1999 *Phys. World* **2** 33
[8] Lebedev O I, van Tendeloo G, Amelinckx S, Leibold B and Habermeier H U 1998 *Phys. Rev.* B **58** 8065
[9] Gu J Y, Kim K H, Noh T W and Suh K S 1995 *J. Appl. Phys.* **78** 6151
[10] Jin S, Tiefel T H, McCormack M, O'Bryan H M, Chen L H, Ramesh R and Schurig D 1995 *Appl. Phys. Lett.* **67** 557
[11] Sánchez R, Vázquez-Vázquez C J R, López-Quintela A, Causa M, Tovar M and Oseroff S 1996 *Appl. Phys. Lett.* **68** 134
[12] Sanchez R D, Rivas J, Vázquez-Vázquez C, Causa M T, Tovar M and Oseroff S B 1997 *Mater. Sci. Forum* **235–8** 831
[13] Vázquez-Vázquez C, López-Quintela M A, Sanchez R D, Caeiro D, Rivas J and Oseroff S B 1998 *Mater. Sci. Forum* **278–81** 606
[14] Vázquez-Vázquez C, Blanco M, López-Quintela M, Sánchez R, Rivas J and Oseroff S 1998 *J. Mater. Chem.* **8** 991
[15] Gupta A and Sun J Z 1999 *J. Magn. Magn. Mater.* **200** 24

[16] Weast R C (ed) *Handbook of Chemistry and Physics* 1955/6 (Boca Raton, FL: Chemical Rubber Company Press)
[17] Kurucz R L and Bell B 1995 *Atomic Line Data* (Kurucz CD-ROM No 23) (Cambridge, MA: Smithsonian Astrophysical Observatory)
[18] Cullity B D 1978 *Elements of X-ray Diffraction* 2nd edn (Reading, MA: Addison-Wesley)
[19] Töpfer J and Goodenough J B 1997 *J. Solid State Chem.* **130** 117
[20] Dyer P E, Issa A and Key P H 1990 *Appl. Phys. Lett.* **57** 186
[21] Girault C, Damiani D, Aubreton J and Catherinot A 1989 *Appl. Phys. Lett.* **54** 2035
[22] Dyer P E, Issa A and Key P H 1990 *Appl. Surf. Sci.* **46** 89
[23] El-Astal A H, Ikram S, Morrow T, Graham W G and Walmsley D G 1995 *J. Appl. Phys.* **77** 6572
[24] Chen K R, King T C, Hes J H, Leboeuf J N, Geohegan D B, Woo R F, Puretzky A A and Donato J M 1999 *Phys. Rev.* B **60** 8373
[25] Huhtinen H, Järvinen J, Laiho R, Paturi P and Raittila J 2001 *J. Appl. Phys.* **90** 1521
[26] Geohegan D B 1992 *Appl. Phys. Lett.* **60** 2732
[27] Gonzalo J, Afonso C N and Ballesteros J M 1997 *Appl. Surf. Sci.* **109/110** 606
[28] Kumuduni W K A, Nakayama Y, Okada T and Maeda M 1993 *J. Appl. Phys.* **74** 7510
[29] Leboeuf J N, Chen K R, Donato J M, Geohegan D B, Liu C L, Puretzky A A and Wood R F 1996 *Appl. Surf. Sci.* **96–8** 14
[30] Bulgakov A V and Bulgakova N M 1995 *J. Appl. Phys.* D **28** 1710
[31] Bulgakov A V and Bulgakova N M 1998 *J. Appl. Phys.* D **31** 693
[32] Lecoeur P, Gupta A, Duncombe P R, Gong G Q and Xiao G 1996 *J. Appl. Phys.* **80** 513
[33] Dang H J, Zhou M F and Qin Q Z 1998 *Appl. Spectrosc.* **52** 1154
[34] Harilal S S, Bindhu C V, Nampoori V P N and Vallabhan C P G 1998 *Appl. Spectrosc.* **52** 449
[35] Gores J, Kung P J, Fenner D B and Budnick J I 1997 *Rev. Sci. Instrum.* **68** 170
[36] Wiedeman L and Helvajian H 1991 *J. Appl. Phys.* **70** 4513
[37] Chrisey D B and Hubler G K 1994 *Pulsed Laser Deposition of Thin Films* (New York: Wiley)
[38] Chen F F 1976 *Introduction to Plasma Physics* (New York: Plenum)
[39] Weimer W A 1988 *Appl. Phys. Lett.* **52** 2171
[40] Gupta A 1993 *J. Appl. Phys.* **73** 7877
[41] Misra A, Mitra A and Thareja R K 1999 *Appl. Phys. Lett.* **74** 929
[42] Marine W, Movtchan I, Simakine A, Patrone L, Dreyfus R, Sentis M, Autric M and Merc N 1996 *MRS Symp. Proc.* **397** 365
[43] Geohegan D B, Puretzky A A and Rader D J 1999 *Appl. Phys. Lett.* **74** 3788
[44] de Gennes P G 1960 *Phys. Rev.* **118** 141
[45] Ju H L, Gopalakrishnan J, Peng J L, Li Q, Xiong G C, Venkatesan T and Greene R L 1995 *Phys. Rev.* B **51** 6143
[46] Park J H, Vescovo E, Kim H J, Kwon C, Ramesh R and Venkatesan T 1998 *Phys. Rev. Lett.* **81** 1953